ACS APPLIED MATERIALS & INTERFACES

Research Article

www.acsami.org

Enhanced Performance of Semitransparent Inverted Organic Photovoltaic Devices via a High Reflector Structure

Dan-Dan Zhang,[†] Xiao-Chen Jiang,[†] Rong Wang,[†] Hao-Jun Xie,[†] Guo-Fu Ma,[†] Qing-Dong Ou,[†] Yuan-Li Chen,[†] Yan-Qing Li,*[,†] and Jian-Xin Tang*[,†]

[†]Institute of Functional Nano and Soft Materials (FUNSOM) & Collaborative Innovation Center of Suzhou Nano Science and Technology, Soochow University, Suzhou 215123, China

Supporting Information

ABSTRACT: Significantly enhanced performances of semitransparent inverted organic photovoltaic devices have been realized by simply introducing a high reflector structure, which comprises several pairs of MoO_3/LiF with a thickness of 60 nm for MoO_3 and 90 nm for LiF, respectively. After optimizing the reflector structure, the enhanced light harvesting is achieved, and thus the increased optical current is obtained. The short-circuit current density (J_{SC}) and power conversion efficiency (PCE) are increased to 10.9 mA cm^{-2} and 4.32%, compared to 8.09 mA cm^{-2} and 3.36% in the control device. This leads to a 30% enhancement in PCE. According to the experimental and simulated results, the improved performance is attributed to the effective reflection of light at the wavelength from 450 to 600 nm, which corresponds to the absorption range of the active layer. The demonstrated light-trapping approach is expected to be an effective method to realize the high efficiency in semitransparent organic photovoltaic devices.

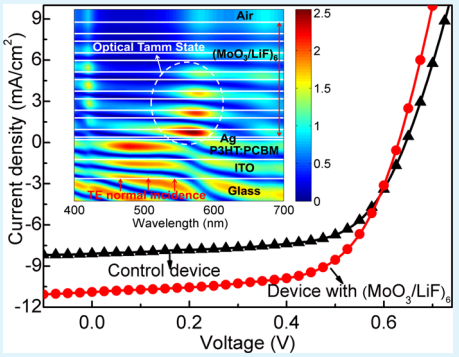

KEYWORDS: *semitransparent electrode, reflector structure, organic photovoltaic devices, light trapping, high transparency, MoO_3/LiF*

1. INTRODUCTION

Organic photovoltaics (OPVs) have attracted a lot of attention as a promising source of renewable energy. In the past few years, many efforts have been devoted to develop the structures and materials of the OPVs owing to their superior advantages such as potential low cost, light weight, and unique flexibility in large area electronic devices.[1−4] However, the low power conversion efficiency (PCE) is still a key issue in realizing commercial OPV technologies. Usually, the PCE is limited by several factors, such as the short exciton diffusion length, the low carrier mobility, and the narrow absorption range.[5,6] Among them, enlarging the absorption range in the solar spectrum is one of the most effective ways to increase the PCE.[7,8] Recently, tandem OPVs exhibits a promising potential in realizing the highly efficient OPV, in which multiple subcells with different energy gaps are stacked to absorb different wavelength ranges to utilize the solar spectrum more effectively. So it is obvious that a semitransparent subcell is indispensable in the tandem OPV, which is used to transmit light to the other subcell and play an important role in the light absorption.[9−11] Furthermore, semitransparent OPVs (STOPVs) are useful in some special applications, such as energy0harvesting windows in a car, foldable curtains, architectural building elements, and clothes, etc.[12] Usually, a good STOPV needs not only a high absorption in its own absorption range but also a high transparency in the complementary wavelength. Compared to the conventional OPVs, one of the key issues in the preparation of STOPVs is related to the transparent top electrode. To obtain a highly transparent top electrode, the reflectance of the electrode is usually low, which will result in a weaker absorption of the active layer and a lower efficiency compared to that of the conventional device with a high reflectance metal electrode.[12−15] Therefore, an appropriate semitransparent electrode is one of the most important issues for the light trapping of STOPV.

Up to now, a variety of semitransparent electrode structures have been developed. First, some ultrathin metal film is used as a semitransparent electrode, but the transmittance is low due to the absorption losses.[16−18] Then some stacked and multilayer electrode structure is employed to achieve the high transmittance; however, the absorption efficiency of the active layer is still low due to the low reflectance of the electrode and leads to a low PCE.[19,20] Accordingly, it is important to give a consideration to both the high transparency and the high reflectance to realize an ideal STOPV. As we know, the transition metal oxide, molybdenum oxide (MoO_3), is a potential candidate for light coupling material and the buffer layer in organic light-emitting diodes (OLEDs) and OPVs due to its high dielectric constant (n, 2.13 at 500 nm), high transmittance, low electrical resistivity, and low evaporating temperature.[21−25] In view of the n matching condition in designing a high reflection multistack structure, a large n difference between two materials is needed to minimize the layers, and it is no doubt that MoO_3 is one of the best

Received: July 18, 2013
Accepted: September 23, 2013
Published: September 23, 2013

candidates for its much higher n than the other common oxides, such as WO_3 and V_2O_5. Here, lithium fluoride (LiF) is selected as the low n (1.386 at 500 nm) material, and a simple but highly effective route is designed to enhance the PCE of STOPV by light trapping and photon recycling via the high reflection of multistacks of MoO_3/LiF (ML). We fabricate an inverted STOPV by depositing six units of ML on top of the Ag anode, achieving a remarkably increased short-circuit current density. As a result, the PCE is increased to 4.32% compared to 3.1% in the control device, which corresponds to about 30% enhancement.

2. EXPERIMENTAL DETAILS

2.1. Fabrication of Semitransparent Inverted OPVs. The semitransparent inverted OPVs were fabricated on ITO-coated glass substrates with a sheet resistance of ~20 Ω/sq, which were ultrasonically cleaned in sequence with detergent, acetone, ethanol, and DI water. The device structure consists of ITO/ZnO/P3HT:PCBM/MoO_3(5 nm)/Ag(20 nm)/$(MoO_3/LiF)_x$; for comparison, the control device without $(MoO_3/LiF)_x$ is also fabricated. The synthesis process of the zinc oxide (ZnO) precursor was modified from the sol−gel method. The 0.5 M zinc acetate and 0.5 M monoethanolamine were dissolved in 2-methoxyethanol with vigorous stirring for 12 h for the hydrolysis reaction at ambient conditions. The sol−gel-derived ZnO layer was formed by spin-coating the prior-prepared ZnO precursor solution onto the UV−ozone treated ITO glass at a speed of 4000 rpm for 40 s and then thermally annealed at 150 °C for 5 min in ambient air, in which a dense ZnO film was formed by hydrolysis. The samples were then moved into a nitrogen-filled glovebox for spin-coating the mixture of poly(3-hexylthiophene) (P3HT) and [6,6]-phenyl-C_{61}-butyric acid methyl ester (PCBM) with a weight ratio of 1:0.8 (10 mg mL^{-1}, dissolved in dichlorobenzene) at 600 rpm for 1 min, which is the optimized condition in our group, and the thickness is about 110 nm.[26] The wet film was subjected to solvent annealing at room temperature and thermal annealing at 110 °C for 10 min inside the glovebox. Subsequently, the samples were transferred to the evaporation chamber with a base pressure of 2×10^{-6} Torr, and 5 nm thick MoO_3 and 20 nm thick Ag were thermally evaporated on the top of P3HT:PCBM as the anode buffer layer and the anode, respectively. The effective area of the device was 0.1 cm^2 confirmed by the overlap of the electrodes. Lastly, the stack layer of MoO_3 (60 nm)/LiF (90 nm) with various cells was deposited onto the top anode as the reflecting layer. The deposition rate and film thickness were monitored with a quartz crystal sensor.

2.2. Characterization of Semitransparent Inverted OPVs. Photovoltaic measurements of semitransparent inverted PSCs without any encapsulation were conducted in air ambience by employing a programmable Keithley 2612 source under illumination of a 150 W Newport 91160 solar simulator using an air mass (AM) 1.5G filter. The simulated light intensity was 100 mW cm^{-2} calibrated by a standard Si optical power meter. The incident photon to current conversion efficiency (IPCE) spectrum was measured with a photomodulation spectroscopic setup (Newport monochromator). The transmission spectrum was measured using an UV/vis/near-IR spectrometer (Perkin-Elmer Lambda 750). All measurements were performed at room temperature.

2.3. Theoretical Calculation. The electric field distribution of the device with or without the ML was simulated by the finite difference time-domain (FDTD) method.[27,28] The refractive indices of ITO, P3HT:PCBM, Ag, MoO_3, and LiF were measured by an α-SE spectroscopic ellipsometer.

3. RESULTS AND DISCUSSION

3.1. Device Structure. To design an appropriate reflector structure to increase the light reflection, we calculate the Bragg forbidden band by solving the well-known equation $|\cos K\Lambda| > 1$ which is based on the Yeh forbidden band theory.[29] The concrete expression is as follows

$$\cos K\Lambda = \cos k_{1x}d_1 \cos k_{2x}d_2 - \frac{1}{2}\left[\frac{k_{1x}}{k_{2x}}\left(\frac{n_2}{n_1}\right)^{2s} + \frac{k_{2x}}{k_{1x}}\left(\frac{n_1}{n_2}\right)^{2s}\right]\sin k_{1x}d_1 \sin k_{2x}d_2 \quad (1)$$

where $k_0 = 2\pi/\lambda$; $k_{1x} = k_0(n_1^2 - n_{\text{eff}}^2)^{1/2}$; $k_{2x} = k_0(n_2^2 - n_{\text{eff}}^2)^{1/2}$; λ is the wavelength; n_{eff} is the tangential effective refractive index of the incidence; n_1 and n_2 are the refractive indices of the MoO_3 and LiF; d_1 and d_2 are the thickness of the MoO_3 and LiF; K is the Bloch wavenumber; Λ is the period of the ML; and $s = 1$ and $s = 0$ are for the TM and TE polarization, respectively. In the calculation, the light is supposed to be normal-incidence, so n_{eff} is zero and the Bragg forbidden band is the same for TM and TE polarization. According to the device structure, the central position of the Bragg forbidden band should be located at ~500 nm which is the absorption peak of P3HT:PCBM. Thus, the position of the Bragg forbidden band is adjusted continuously by changing the thickness of MoO_3 and LiF with an assumption that the pair number (N_P) of MLs is infinite. Lastly, the optimum thickness of MoO_3 and LiF is obtained as 60 and 90 nm, respectively, while the central wavelength of the Bragg forbidden band is just at 500 nm (as shown in Figure 1).

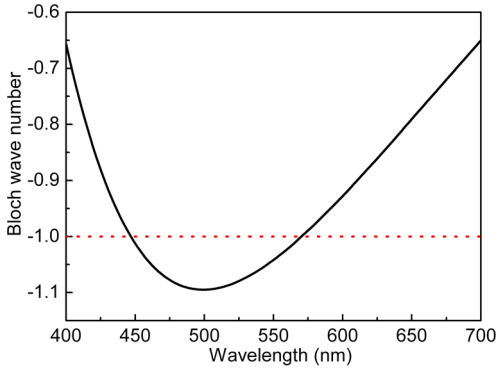

Figure 1. Calculated Bloch wavenumber distribution at the visible wavelength.

To clarify the exact value of N_P of ML, the calculated reflectance and transmittance of the stacked structures with different pairs of MLs are displayed in Figure 2(a) and (b). It is found that the reflectance is increased sharply with the increase of N_P at the wavelength from 450 to 600 nm, which matches with the absorption spectrum of P3HT:PCBM. A much higher reflectance of 80% and 96% is observed, while N_P is 4 and 6, respectively, in contrast with only 51% for the 20 nm thick Ag film. A further increase in N_P does not cause a remarkable change in the reflectance, and the corresponding transmittance for all samples shows the contrary law. Consequently, we can infer that the maximum of N_P with a value of 6 is enough to achieve a high reflectance, which is approaching to 100%. On account of the relationship between the thickness of the functional layer and the value of N_P, the total absorption enhancement (TAE) of the device with six pairs of MoO_3/LiF is calculated by following the literature.[30] As shown in Figure 2(c), the TAE reaches the maximum, while the thickness of P3HT:PCBM is 105 nm, which is very close to our optimized

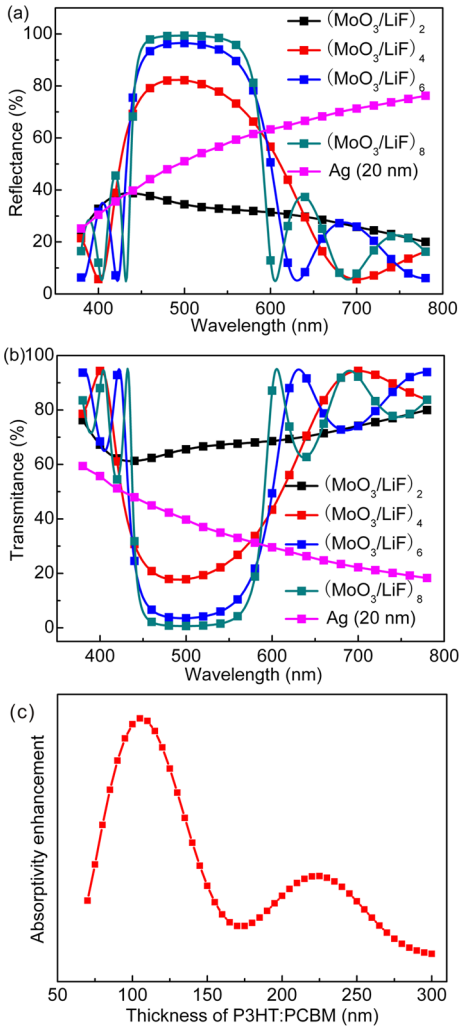

Figure 2. (a) Reflectance spectra and (b) the transmittance spectra of the films of $(MoO_3/LiF)_2$, $(MoO_3/LiF)_4$, $(MoO_3/LiF)_6$, and $(MoO_3/LiF)_8$ and the 20 nm thick Ag. (c) The simulated total absorption enhancement of the device with $(LiF/MoO_3)_6$ at the different active layer thickness.

thickness (110 nm). The TAE value at 110 nm is only a bit lower than its maximum, suggesting that six pairs of ML are just suitable for the optimized active thickness to achieve the largest enhancements. So the device structure can be designed as the picture described in Figure 3

3.2. Device Photovoltaic Charateristics. The current density−voltage (J−V) curves of the devices based on different pairs of ML are plotted in Figure 4 under AM 1.5G irradiation at an intensity of 100 mW cm^{-2}. For comparison, the control device without the ML layer was also fabricated using identical process parameters during the same batch processing, and the corresponding J−V properties are also shown in Figure 4. It can be observed that there is a significant increase in short-circuit current density (J_{SC}) of the devices upon the incorporation of the ML layer, and the resulting PCE is enhanced. A maximum increase of J_{SC} and PCE of 10.9 mA cm^{-2} and 4.32% are obtained while N_P reaches 6, as compared to 8.09 mA cm^{-2} and 3.36% for the control device. Besides, the fill factor (FF) is also increased slightly owning to the improved J_{SC}, while the open-circuit voltage (V_{OC}) remains almost unchanged for all of the devices due to the unchanged organic−electrode interface nature. The detailed features of the corresponding devices are listed in Table 1. These results indicate that the PCE with ∼30% improvement is mainly ascribed to the increase of light absorption related to the high reflection, which is approximating to 100% via the ML demonstrated in Figure 2.

To get additional insight into the improvement in the J_{SC}, the incident photon to current conversion efficiency (IPCE) spectra of the corresponding devices are compared in Figure 5(a). It is noted that the IPCE of the devices with the ML layer is enhanced significantly in a broad wavelength range of 450−600 nm in comparison with that of the control device, which corresponds to an increase of about 20%, while the difference in shape of the spectra is negligible. Hence we can infer that the expected improvement in the device performance is attributed to the reflected light by the stacked ML layer, which can transmit the 20 nm Ag semitransparent anode and be absorbed again by the active layer. On the contrary, a lot of lights will be lost in the control device because a relevant portion of the lights transmits the Ag semitransparent anode into the air due to its high transmission of ∼40% at 500 nm (shown in Figure 2(b)). Furthermore, we also characterize the total device transmittance as illustrated in Figure 5(b). The device with six pairs of ML has the lowest transmittance at the wavelength from 450 to 600 nm, followed by the device with four pairs of ML, and the control device has the highest transmittance to maintain a semitransparent property. However, in consideration of the other wavelength from 600 to 800 nm, the devices with ML show a higher transmittance over 40%, which could effectively guarantee the semitransparent properties of the devices.

Moreover, to better clarify the device properties discussed above, we also measured the J−V characteristic of the normal device (no transparent device) with a thick Ag (100 nm) anode (not shown here). It is found that PCE is only 3.9%, which is lower than that of the device with Ag (20 nm)/$(ML)_6$, so it is reasonable that the Ag (20 nm)/$(ML)_6$ anode is more competent for the high-efficiency device. Importantly, the Ag (20 nm)/$(ML)_6$ anode can also keep the semitransparent properties of the device, while the 100 nm thick Ag anode cannot do this. In a word, we proved a potential way to achieve the highly efficient STOPV by introducing a high reflection layer to reflect the light in the range of 450−600 nm which can be absorbed by the active layer and to transmit the light located in the complementary wavelength of 600−780 nm. Figure S1 (Supporting Information) also shows the calculated transmittance of the optimized device, which is consistent with the experimental result.

3.3. Theoretical Calculation. To further illustrate the increased J_{SC} resulting from the light trapping via the reflection of the ML layer, the electric field distribution of the device with six pairs of ML and the control device were simulated by the FDTD method. As described in Figure 6(b), the field intensity especially in the P3HT:PCBM layer for the device with ML is much stronger than that of the control device in Figure 6(a). It is obvious that the enhancement region of the optical electric field is mainly distributed in the wavelength of 450−600 nm, which agrees with the absorption wavelength of the active layer, and these results are in favor of our analysis above. In addition, an optical Tamm state is also formed in the ML layer, which can be excited directly from the free space incidence without the assistance of nanopatterned structures.[31−33] So we can get the conclusion that the high reflection of the ML layer can indeed trap the light that can be reabsorbed by the active layer and produce much more excitons to increase the J_{SC} and PCE.

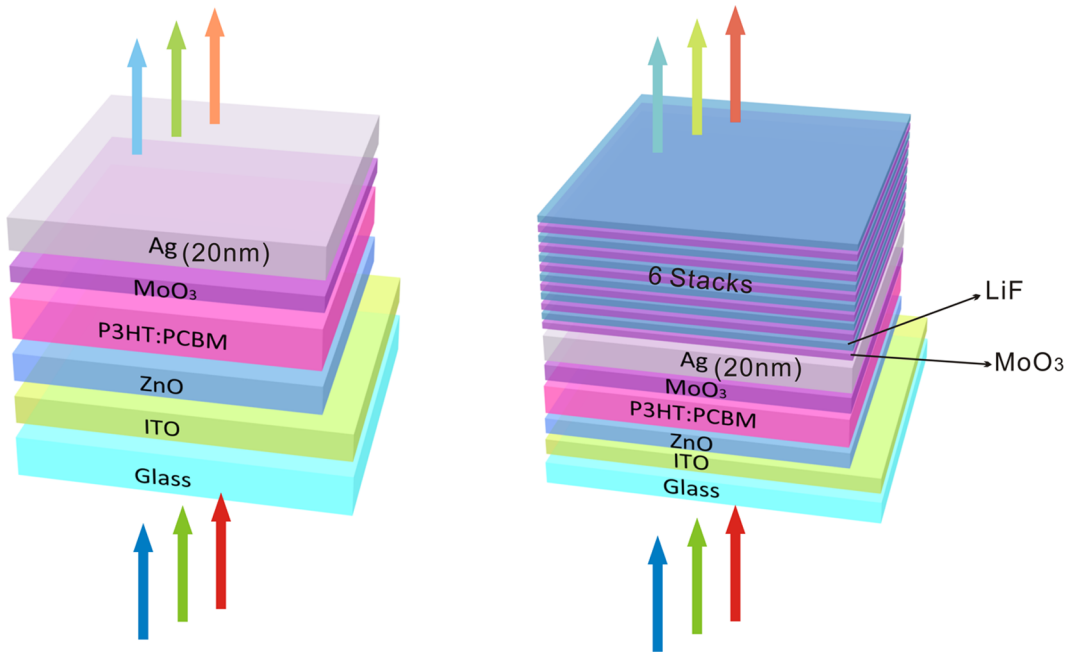

Figure 3. Structures of the control device (left) and the device with $(MoO_3/LiF)_6$ (right).

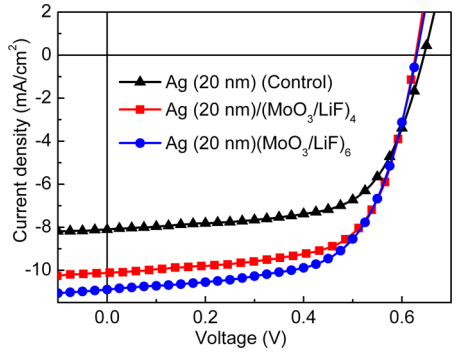

Figure 4. *J*–*V* characteristics of the devices with the semitransparent anode of Ag, Ag/$(MoO_3/LiF)_4$, and Ag/$(MoO_3/LiF)_6$ under the irradiation of AM1.5G, 100 mW cm^{-2}.

Table 1. Performance Parameters of the Devices with Ag, Ag/$(MoO_3/LiF)_4$, and Ag/$(MoO_3/LiF)_6$ Semitransparent Anode

device	V_{OC} (V)	J_{SC} (mA cm^{-2})	FF (%)	PCE (%)
control	0.64	8.09	64	3.36
$(MoO_3/LiF)_4$	0.62	10.1	66	4.16
$(MoO_3/LiF)_6$	0.63	10.89	66	4.32

In addition, to synthetically estimate the repeatability of our devices, the statistics graph of PCEs for the control and optimized devices is fitted by the Gaussian distribution shown in Figure 6(c), indicating that there exists no overlap between process 1 (blue ~3.36) and 2 (red ~4.32), indicating process 2 is obviously the cause of the improved PCEs. Also the narrow distribution and considerable repeated frequency of each process give a great viability for our work to be reproduced.

4. CONCLUSIONS

In conclusion, we have demonstrated a promising method to effectively trap the light for the semitransparent inverted OPVs by simply incorporating the reflector structure. We scheme out

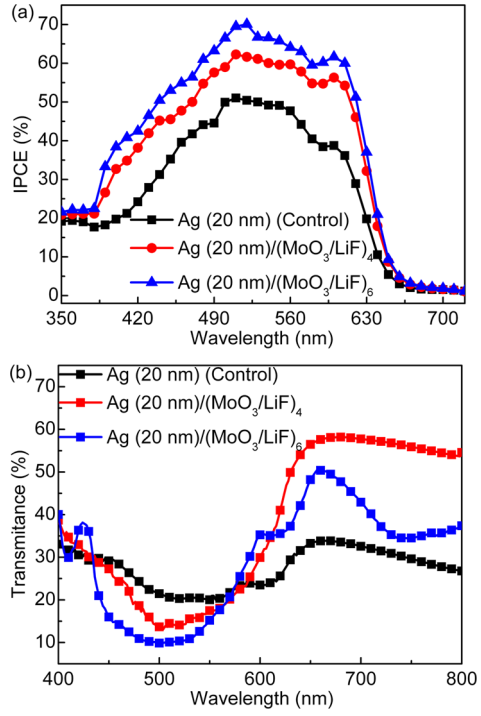

Figure 5. (a) IPCE characteristics and (b) the transmittance spectra of the devices with the semitransparent anode of Ag, Ag/$(MoO_3/LiF)_4$, and Ag/$(MoO_3/LiF)_6$.

a reasonable reflector with a structure of Ag (20 nm)/$(ML)_6$ by calculating the Bragg forbidden band and the refection. The enhancements in J_{SC} and PCE are achieved without affecting the V_{OC}, and the FF is also improved somewhat. Interestingly, the PCE is even higher than that of the opaque device with a thick Ag anode (100 nm), implying that the Ag (20 nm)/$(ML)_6$ anode is more competent for the high-efficient device without sacrificing the device transmittance. The operating mechanisms of the ML are further systematically investigated

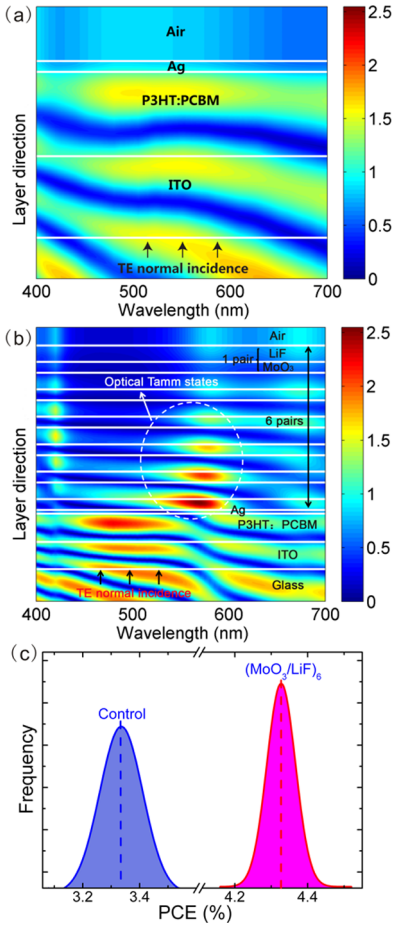

Figure 6. Electric field distribution of the device with a (a) Ag anode and (b) Ag/$(MoO_3/LiF)_6$ anode and (c) distribution of device power conversion efficiencies (PCEs) for the control device and the modified one with $(MoO_3/LiF)_6$.

by the IPCE measurements and theoretical calculations, which reveal that the improvement in performance is mainly due to the increased light absorption by the active layer relating to the high reflection via the ML without influencing the device transmittance at the other visible wavelength. The method reported here provides a facile approach to achieve high-performance semitransparent OPVs.

■ ASSOCIATED CONTENT

Supporting Information

Additional figures showing the measured and simulated transmittance of the device with $(MoO_3/LiF)_6$ and the $J-V$ characteristics of the control device with and without white paper on the semitransparent Ag anode. This material is available free of charge via the Internet at http://pubs.acs.org.

■ AUTHOR INFORMATION

Corresponding Authors

*E-mail: yqli@suda.edu.cn. Tel. & Fax: +86-512-65880941.
*E-mail: jxtang@suda.edu.cn. Tel.: +86-512-65880942.

Notes

The authors declare no competing financial interest.

■ ACKNOWLEDGMENTS

The authors gratefully acknowledge the financial support from the 973 program (No. 2014CB932600), the NSFC (Grant Nos. 61205033, 91027041, 612111116, 61007020, 61107022), the Natural Science Foundation of Jiangsu Province (No. BK2011280), Bureau of Science and Technology of Suzhou Municipality (Nos. SYG201237 and SYG 201232), and PAPD.

■ REFERENCES

(1) Li, G.; Zhu, R.; Yang, Y. *Nat. Photon.* **2012**, *6*, 153−161.
(2) He, Z. C.; Zhong, C. M.; Su, S. J.; Xu, M.; Wu, H. B.; Cao, Y. *Nat. Photon.* **2012**, *6*, 591−595.
(3) You, J.; Dou, L.; Yoshimura, K.; Kato, K.; Ohya, K.; Moriarty, T.; Emery, K.; Chen, C. C.; Gao, J.; Li, G.; Yang, Y. *Nat. Commun.* **2013**, *4*, 1446.
(4) Yang, B. B.; Zhang, D. D.; Lee, S. T.; Li, Y. Q.; Tang, J. X. *Appl. Phys. Lett.* **2013**, *102*, 073301.
(5) Xu, Y.; Shen, L.; Yu, W. J.; Zhang, H. F.; Chen, W. Y.; Ruan, S. P. *IEEE Electron Device Lett.* **2012**, *33*, 1027−1029.
(6) Guo, X. Y.; Liu, F. M.; Yue, W.; Xie, Z. Y.; Geng, Y. H.; Wang, L. X. *Org. Electron.* **2009**, *10*, 1174−1177.
(7) Lee, Y. Y.; Tu, K. H.; Yu, X. X.; Tan, Li. S. S.; Hwang, J. Y.; Lin, C. C.; Chen, K. H.; Chen, L. C.; Chen, C. W. *Nano Lett.* **2011**, *5*, 6564−6570.
(8) Kim, Y. H.; Meskamp, L. M.; Zakhidov, A. A.; Sachse, C.; Meiss, J.; Bikova, Julia.; Cook, A.; Zakhidov, A. A.; Leo, K. *Sol. Energy Mater. Sol. Cells* **2012**, *96*, 244−250.
(9) Xue, J.; Uchida, S.; Rand, B. P.; Forrest, S. R. *Appl. Phys. Lett.* **2004**, *85*, 5757.
(10) Dennler, G.; Prall, H. J.; Koeppe, R.; Eggiger, M.; Autengruber, R.; Sariciftci, N. S. *Appl. Phys. Lett.* **2006**, *89*, 073502.
(11) Shrotriya, V.; Wu, E. H. E.; Li, G.; Yao, Y.; Yang, Y. *Appl. Phys. Lett.* **2006**, *88*, 064104.
(12) Han, D.; Kim, H.; Lee, S.; Seo, M.; Yoo, S. *Opt. Express* **2010**, *18*, 513−521.
(13) Kim, H. P.; Lee, H. J.; Jang, J. *Sol. Energy Mater. Sol. Cells* **2013**, *108*, 38−43.
(14) Ng, G. M.; Kietzke, E. L.; Kietzke, T.; Tan, L. W.; Liew, P. K.; Zhu, F. R. *Appl. Phys. Lett.* **2007**, *90*, 103505.
(15) Schmidt, H.; Flügge, H.; Winkler, T.; Bülow, T.; Riedl, T.; Kowalsky, W. *Appl. Phys. Lett.* **2009**, *94*, 243302.
(16) Oyamada, T.; Sugawara, Y.; Terao, Y.; Sasabe, H.; Adachi, C. *Jpn. J. Appl. Phys* **2007**, *46*, 1734−1735.
(17) Li, G.; Chu, C. W.; Shrotriya, V.; Huang, J.; Yang, Y. *Appl. Phys. Lett.* **2006**, *88*, 253503−253505.
(18) Huang, J.; Li, G.; Yang, Y. *Adv. Mater.* **2008**, *20*, 415−419.
(19) O'Connor, B.; An, K. H.; Pipe, K. P.; Zhao, Y. Y. Y.; Shtein, M. *Appl. Phys. Lett.* **2006**, *89*, 233502.
(20) Tao, C.; Ruan, S. P.; Zhang, X. D.; Xie, G. H.; Shen, L.; Kong, X. Z.; Dong, W.; Liu, C. X.; Chen, W. Y. *Appl. Phys. Lett.* **2008**, *93*, 193307.
(21) Xie, G. H.; Meng, Y. L.; Wu, F. M.; Tao, C.; Zhang, D. D.; Liu, M. J.; Xue, Q.; Chen, W.; Zhao, Y. *Appl. Phys. Lett.* **2008**, *92*, 093305.
(22) Liu, J.; Shao, S. Y.; Fang, G.; Meng, B.; Xie, Z. Y.; Wang, L. X. *Adv. Mater.* **2012**, *24*, 2774−2779.
(23) Zhang, D. D.; Feng, J.; Zhong, Y. Q.; Liu, Y. F.; Wang, H.; Jin, Y.; Bai, Y.; Chen, Q. D.; Sun, H. B. *Org. Electron.* **2010**, *11*, 1891−1895.
(24) Sun, F. Z.; Shi, A. L.; Xu, Z. Q.; Wei, H. X.; Li, Y. Q.; Lee, S. T.; Tang, J. X. *Appl. Phys. Lett.* **2013**, *102*, 133303.
(25) Tao, C.; Xie, G. H.; Liu, C. X.; Zhang, X. D.; Dong, W.; Meng, F. X.; Kong, X. Z.; Shen, L.; Ruan, S. P.; Chen, W. Y. *Appl. Phys. Lett.* **2009**, *95*, 053303.
(26) Sun, F. Z.; Shi, A. L.; Xu, Z. Q.; Wei, H. X.; Li, Y. Q.; Lee, S. T.; Tang, J. X. *Appl. Phys. Lett.* **2013**, *102*, 133303.
(27) Gu, Y.; Zhang, D. D.; Ou, Q. D.; Deng, Y. H.; Zhu, J. J.; Cheng, L.; Liu, Z.; Lee, S. T.; Li, Y. Q.; Tang, J. X. *J. Mater. Chem. C* **2013**, *1*, 4319−4326.

(28) Mahmoud, M. A.; Poncheri, A. J.; Phillips, R. L.; El-Sayed, M. A. *J. Am. Chem. Soc.* **2010**, *132*, 2633.
(29) Yeh, P.; Yariv, A.; Hong, C. S. *J. Opt. Soc. Am.* **1977**, *67*, 423−438.
(30) Min, C.; Li, J.; Veronis, G.; Lee, J. Y.; Fan, S. H.; Peumans, P. *Appl. Phys. Lett.* **2010**, *96*, 133302.
(31) Zhang, X. L.; Song, J. F.; Li, X. B.; Feng, J.; Sun, H. B. *Appl. Phys. Lett.* **2012**, *101*, 243901.
(32) Kaliteevski, M.; Iorsh, I.; Brand, S.; Abram, R. A.; Chamber-lain, J. M.; Kavokin, A. V.; Shelykh, I. A. *Phys. Rev. B* **2007**, *76*, 165415.
(33) Zhang, X. L.; Song, J. F.; Li, X. B.; Feng, J.; Sun, H. B. *Org. Electron.* **2013**, *14*, 1577−1585.